Structural systematics of aryl-1,3-dithiane derivatives: crystal and energy-minimised structures, and Hirshfeld surface analysis

Julio Zukerman-Schpector,[I*] Lucas Sousa Madureira,[I] Hélio A. Stefani,[II] Olga Gozhina[II] and Edward R. T. Tiekink[III*]

[I] Universidade Federal de São Carlos, Laboratório de Cristalografia, Estereodinâmica e Modelagem Molecular, Departmento de Química, 13565-905 São Carlos, SP, Brazil

[II] Universidade de São Paulo, Departamento de Farmácia, Faculdade de Ciências Farmacêuticas, 05508-900 São Paulo-SP, Brazil

[III] Sunway University, Centre for Crystalline Materials, Faculty of Science and Technology, 47500 Bandar Sunway, Selangor Darul Ehsan, Malaysia

Received; accepted

Keywords: Aryl-1,3-thianes / conformation / DFT / crystal structure analysis / X-ray diffraction

Abstract. The crystal structure analysis of three aryl-1,3-dithiane derivatives, with aryl = 4-methylphenyl (**1**), 4-chlorophenyl (**2**) and 2,4-dichlorophenyl (**3**), shows the three molecules to have very similar conformations, with the aryl ring lying on an approximate mirror plane that bisects the dithiane ring which adopts a chair conformation; the energy-minimised structures are consistent with the experimental structures. The greater barrier to rotation about the methine-C–C(ipso) bond in **3**, cf. **1** and **2**, is related to unfavourable intramolecular S···Cl interactions in the putative transition state. The molecular packing in **1**–**3**, while globally similar, are distinct, being based on combinations of identifiable C–H···π(arene), C–H···S and C–Cl···π(arene) interactions. The lack of isostructural relationships points to the significance of the identified intermolecular interactions to direct molecular packing.

* Correspondence authors: julio@power.ufscar.br (J.Z-S.) and edwardt@sunway.edu.my (E.R.T.T.)

Introduction

While the primary goal of crystal engineering in the organic solid-state has been the rational assembly of molecules in crystal structures, in truth, the design of pre-specified three-dimensional architectures remains elusive. On the positive side, hydrogen bonding and the now well-understood halogen bonding can be exploited to reliably assemble molecules owing to their strong interaction energy and directional nature [1-4]. Even though these modes of aggregation will probably form in circumstances when the respective functional groups are present, they are more than likely to simply lead to the formation of small aggregates from which the crystal structure is then constructed, often relying on other, "second tier", intermolecular interactions, such as π···π and C–H···π [5-8]. The above "supramolecular synthon approach" [2] presupposes that specific intermolecular interactions dominate the way molecules form crystals, a conclusion fraught with danger as global crystal packing considerations, e.g. the need to fill space, are likely to be at least as important, especially in the absence of strong and directional intermolecular interactions [7-11].

In order to fully understand the interplay between the concepts underlying supramolecular synthons and global packing of molecules, thorough analyses of crystal structures of closely related molecules, i.e. those differing in a limited number of substituents, is required. In this way, the influence of small perturbations in chemistry upon molecular packing can be determined. In keeping with this idea, an emphasis of recent work has been upon the monitoring of the effect of systematically changing the electronegativity of substituents in the aryl rings of two series small organic molecules [12, 13]. For these series, significant electronic effects can be invoked to account for different molecular packing, but the participation of the substituents in specific interactions can also be crucial. As a continuation of these studies, herein the crystal and molecular structures of three aryl-1,3-dithiane derivatives that differ in the nature of the electronegativity of the substituents in the aryl ring are analysed and compared with their energy-minimised structures Fig. 1. As well, their Hirshfeld surfaces have been analysed in order to gain more information on the molecular packing. Molecules **1**–**3** became available during a complementary synthetic study of 1,3-dithianes.

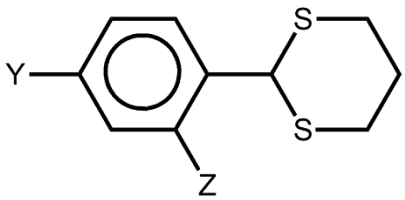

1: Y = Me, Z = H
2: Y = Cl, Z = H
3: Y = Cl, Z = Cl

Fig. 1. Chemical structures of aryl-1,3-diazines investigated herein.

In 1965, Corey and Seebach introduced the use of 1,3-dithianes as important umpolung linchpins in organic synthesis [14, 15]. For over 40 years, this approach has become a mainstay for the union of both simple and complex fragments [16-19]. Among the most important features of these compounds is their stability under both acidic and basic conditions [20, 21] and their potential utility in organic synthesis as acyl carbanion equivalents in carbon-carbon bond forming reactions [14, 20, 21]. A wide range of electrophiles, including alkyl halides, aldehydes, and epoxides, react smoothly with the derived acylanion equivalents [20, 21].

In connection with on-going research interest on the preparation and reactivity of potassium organotrifluoroborate salts, and their use as intermediates in organic synthesis [22-29], various air-stable and storable 1,3-dithiane reagents were synthesised to produce potassium 2-organo-1,3-dithianotrifluoroborate salts to be used in cross-coupling Suzuki-Miyaura reaction. Herein, a comprehensive crystallographic and computational analysis of three of these molecules, Fig. 1, is described along with a comparison with literature structures.

Experimental

Synthesis and crystal growth

The synthesis of **1**-**3** followed literature precedents [30, 31]. Thus, a solution of the corresponding aldehyde (0.037 mol, 1 equiv.) in chloroform (20 mL) was combined with an equimolar amount of propane-1,3-dithiol (3.7 mL, 0.037 mol, 1 equiv.) at room temperature. The solution was stirred for 1 h at this temperature, then cooled down to 253 K and BF_3 etherate (0.46 mL, 0.0037 mol, 0.1 equiv.) was added dropwise. The reaction solution was allowed to warm to room temperature and stirred overnight. After this time, the solution was washed three times each with water, 10% aqueous KOH, water and dried over $MgSO_4$. Crystals of each of **1**-**3** were obtained by slow evaporation of the respective methanol solution.

Crystal structure determination

Intensity data were measured under ambient conditions on a Bruker APEXII CCD diffractometer fitted with Mo Kα radiation. Data processing were accomplished with APEX2 and SAINT [32], and empirical absorptions corrections were applied with SADABS [33]. The structures were solved by direct methods using SIR2014 [34] and refined on F^2 by full-matrix least-squares with anisotropic displacement parameters for all non-hydrogen atoms with the use of SHELXL2014 [35], integrated into WinGX [36]. The C-bound H atoms were placed on stereochemical grounds and refined in the riding model approximation with U_{iso} = 1.2-1.5U_{eq}(carrier atom). A weighting scheme of the form $w = 1/[\sigma^2(F_o^2) + (aP)^2 + bP]$ where $P = (F_o^2 + 2F_c^2)/3$ was introduced. For **2**, the residual electron density peaks of 1.24 and -0.43 eÅ^{-3} were located 1.15 and 0.76 Å, respectively, from

the S3 atom. Unit cell data, X-ray data collection parameters, and details of the structure refinement are given in Table 1. The programs ORTEP-3 for Windows [36], PLATON [37], QMol [38] and DIAMOND [39] were also used in the crystallographic analysis.

Table 1. Crystallographic data and refinement details for **1**–**3**.[1]

	1	**2**	**3**
Formula	$C_{11}H_{14}S_2$	$C_{10}H_{11}ClS_2$	$C_{10}H_{10}Cl_2S_2$
Formula weight	210.34	230.76	265.20
Crystal colour, habit	Colourless prism	Colourless prism	Colourless prism
Crystal size/mm	0.30 x 0.37 x 0.41	0.34 x 0.46 x 0.47	0.27 x 0.31 x 0.39
Crystal system	monoclinic	orthorhombic	orthorhombic
Space group	$P2_1/n$	$Pna2_1$	$P2_12_12_1$
a/Å	5.6457(3)	18.0536(8)	6.7189(5)
b/Å	18.0070(9)	10.3952(5)	12.6743(9)
c/Å	11.1982(5)	5.9019(2)	13.8231(10)
β/°	95.752(3)	90	90
V/Å^3	1132.70(10)	1107.61(8)	1177.14(15)
Z/Z'	4/1	4/1	4/1
D_c/g cm^{-3}	1.233	1.384	1.496
F(000)	448	480	544
μ(Mo$K\alpha$)/mm^{-1}	0.423	0.673	0.864
Measured data	7436	4162	4637
θ range/°	2.2 – 25.4	2.3 – 25.4	2.2 – 25.4
Unique data	2073	1896	2114
R_{int}	0.015	0.021	0.016
Observed data ($I \geq 2.0\sigma(I)$)	1900	1780	2034
R, obs. data; all data	0.038; 0.041	0.066, 0.070	0.027, 0.028
a, b in weighting scheme	0.047, 0.533	0.127, 1.084	0.031, 0.407
R_w, obs. data; all data	0.100; 0.102	0.197, 0.203	0.068, 0.069

[1] Supplementary Material: Crystallographic data (excluding structure factors) for the structures reported in this paper have been deposited with the Cambridge Crystallographic Data Centre as supplementary publication numbers CCDC-1435167-1435169. Copies of available material can be obtained free of charge, on application to CCDC, 12 Union Road, Cambridge CB2 1EZ, UK, (fax: +44-(0)1223-336033 or e-mail: deposit@ccdc.cam.ac.uk). The list of Fo/Fc-data is available from the author up to one year after the publication has appeared.

Computational chemistry

The unrestrained geometry optimisation calculations were performed using the Firefly [40, 41] package at the B3LYP/6-311G++(d,p) level [42-45] with an algorithm based on the Quadratic Approximation (QA) [46] and a threshold gradient value of 10^{-5} a.u. Frequency analyses

were carried out to verify the nature of the stationary structures obtained. The single point energies of the crystallographic (experimental) structures have also been calculated.

The Intrinsic Reaction Coordinate (IRC) calculations were performed using the Gonzalez-Schlegel second-order method [47], with a threshold gradient value of 10^{-5} a.u., and a step-size between points on the reaction path of 0.2 a.u.

The NBO donor-acceptor pairs were checked. The interaction energies were calculated according to second-order stabilisation (E2PRT) and steric exchange energies of NBO analyses [48]. Partial charges have been evaluated by Natural Population Analysis (NPA) model [48].

Finally, structures, charts and surfaces, were drawn using the wxMacMolPlt and JMol software [49, 50].

Results

Experimental molecular structures

The molecular structures of **1**–**3** are shown in Fig. 2 and selected geometric parameters are collated in Table 2. Each structure features a 1,3-dithiane ring, having a chair conformation with the methine- and central methylene-C atoms out of the plane defined by the remaining atoms. The aryl ring is connected equatorially to the 1,3-dithiane ring at the C2 position, i.e. at the methylene link between the sulphur atoms. From the dihedral angle data included in Table 2, it is evident that the aryl ring adopts a conformation perpendicular to the plane through the 1,3-dithiane ring so that each molecule approximates mirror symmetry with the aryl ring as well as the methine- and central-methylene-C atoms lying on the putative plane. In **3**, the methine-H atom is syn with respect to the 2-chloride, enabling the formation of a close intramolecular H2···Cl14 contact of 2.54 Å.

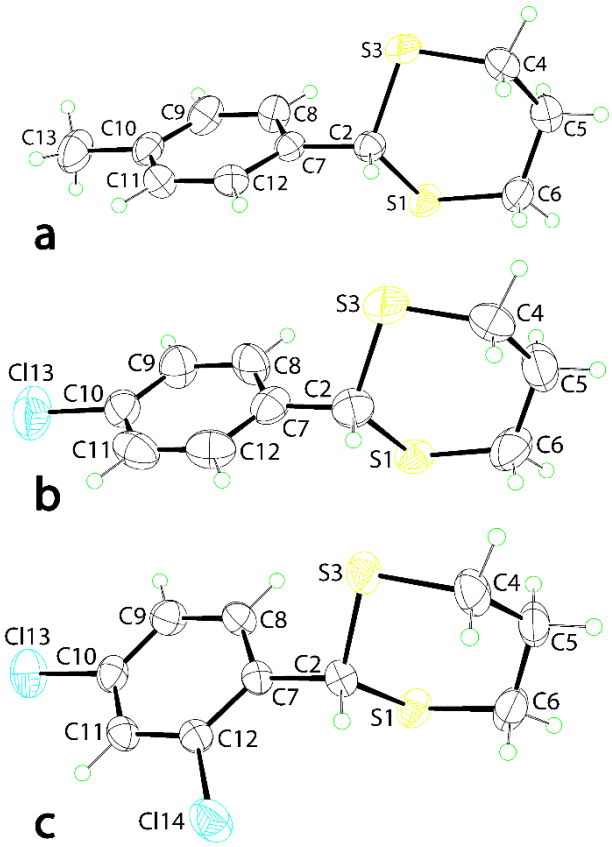

Fig. 2. Molecular structures of **1-3** showing atom labelling scheme. The diagrams are drawn at the 35% probability level.

Table 2. Summary of key geometric parameters (Å, º) for **1**–**3**.

Parameter	**1**	**2**	**3**
C2–S1	1.8096(18)	1.825(8)	1.814(3)
C2–S3	1.8091(19)	1.810(9)	1.816(3)
C6–S1	1.806(2)	1.778(10)	1.814(4)
C4–S3	1.805(2)	1.806(10)	1.807(3)
C2–C7	1.506(2)	1.488(12)	1.501(4)
C2–S1–C6	100.04(10)	101.3(5)	98.83(16)
C2–S3–C4	99.89(10)	100.5(4)	98.93(16)
S1–C2–S3–C4	-58.79(14)	-57.9(6)	-60.9(2)
S3–C2–S1–C6	58.63(13)	55.6(6)	61.1(2)
C2–S1–C6–C5	-58.0(2)	-55.6(11)	-59.7(3)
C2–S3–C4–C5	58.7(2)	59.1(8)	59.2(3)
(S1,C2,S3)/(C7-C12)	89.03(8)	88.0(3)	84.69(13)

There is a high degree of concordance in the salient bond lengths in the three structures and only minor variations in bond angles. The major difference in the molecules relates to the relative orientations of the aryl rings and these are highlighted in the overlay diagram shown in Fig. 3. Also included are images for literature precedents [51-57], i.e. molecules that do not bear groups capable of forming conventional hydrogen bonding interactions, e.g. hydroxyl. Clearly, the molecular structures display similar conformations. The relative orientation of the aryl ring to the 1,3-

dithiane ring can be quantified in terms of the dihedral angle between the C6 ring and the SCS fragment. In **1**–**3**, these vary from a narrow 84.69(13)º in **3** to a wide 89.03(8)º in **1**. These values fall within the limits of the literature structures for which dihedral angles range from 79.10(4)º in the structure with a 2-benzaldehyde group [51] to 89.18(4)º in the 4-nitrophenyl derivative [55].

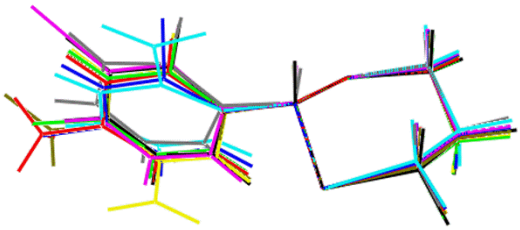

Fig. 3. Overlay diagram of the molecular structures of **1** (red image), **2** (green), **3** (blue), as well as literature precedents: Y = Z = F (grey), Z = H and Y = H (black), Y = NO_2 (olive-green), Y = H, Z = CH(=O) (aqua), and Y = Z = H with 3-Br (pink), 3-NO_2 (yellow). The molecules have been overlapped so that the SCS fragments are coincident.

Molecular packing in 1–3

Despite the similarly in chemical composition of **1**–**3**, molecules crystallise with different crystallographic symmetries, Table 1. The geometric parameters characterising the most prominent points of contact in the molecular packing of **1**–**3** are collected in Table 3. The unit cell contents of **1** feature C–H···π(arene) interactions. The H-donors are derived from methylene- and methyl-groups so that in essence the arene ring is bridging these. The result of these contacts is the formation of an undulating supramolecular layer parallel to (1 0 1) as illustrated in Fig. 4a. Layers thus formed stack with no specific interactions between them, Fig.4b. A view down the *c*-axis is also included, Fig. 4c, to enable a comparison with the molecular packing in **2**.

Table 3. Summary of intermolecular interactions (A–H···B; Å, º) operating in the crystal structures of **1**–**3**.[1]

A	H/Cl	B	A–H	H···B	A···B	A–H···B	Symmetry operation
1							
C4	H4a	Cg(C7-C12)	0.97	2.81	3.651(2)	146	½+*x*, 1½-*y*, ½+*z*
C13	H13c	Cg(C7-C12)	0.96	2.94	3.829(3)	155	-*x*, 1-*y*, 1-*z*
2							
C4	H4a	Cg(C7-C12)	0.97	2.74	3.616(10)	150	1½-*x*, ½+*y*, -½+*z*
C10	Cl13	Cg(C7-C12)	1.736(8)	3.971(5)	4.651(10)	101.9(3)	2-*x*, 1-*y*, ½+*z*
C12	H12	S1	0.93	2.87	3.751(10)	158	x, *y*, 1+*z*
3							
C5	H5b	Cg(C7-C12)	0.97	2.84	3.612(4)	138	1½-*x*, 1-*y*, -½+*z*

[1] Cg corresponds to the ring centroid of the specified atoms.

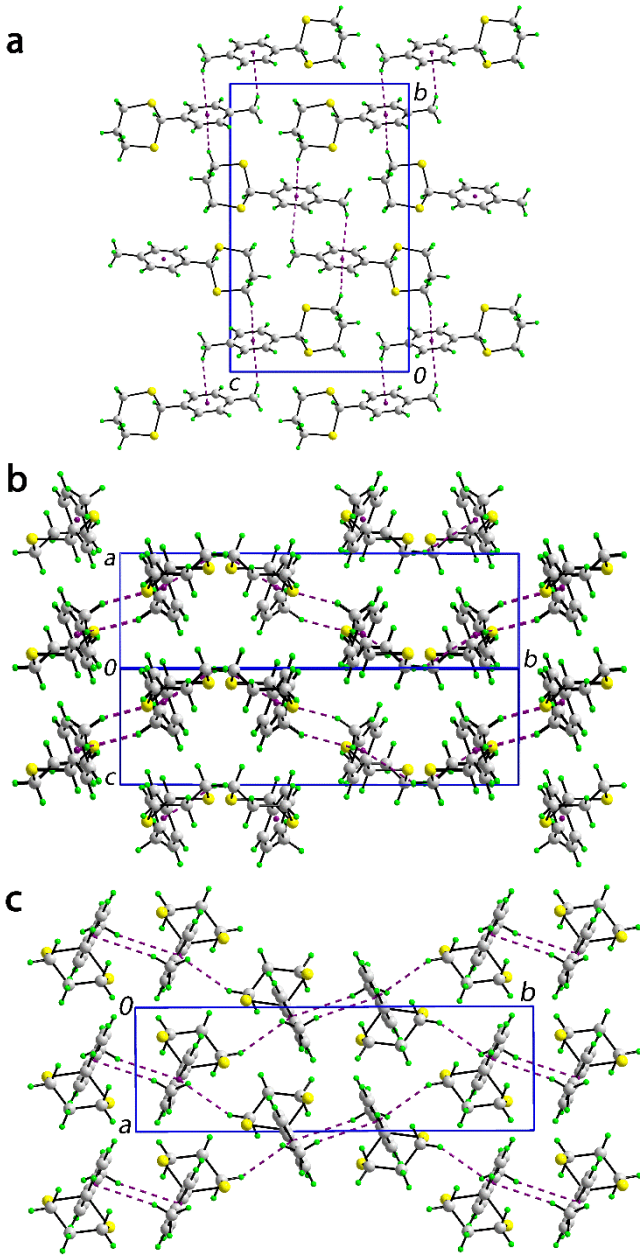

Fig. 4. (a) A plan view of the undulating supramolecular layer in **1** sustained by C–H···π(arene) interactions shown as purple dashed lines, (b) A view highlighting the stacking of layers, and (c) A view in projection down the *c*-axis of the unit cell contents for **1**.

For **2**, the aromatic ring also functions as a supramolecular bridge accepting a methylene-C–H···π(arene) contact, as for **1**, and C–Cl···π(arene) contact. The latter might be considered a "side-on" approach as seen in the C10–Cl13···Cg(C6-C13) angle of 101.9(3)º as opposed to an "end-on" approach where the equivalent angle would be close to 180º. In effect, the methyl-C–H···π(arene) contacts of **1** have been simply substituted by C–Cl···π(arene) interactions in **2**. The side-on approach does have a consequence in that the aforementioned interactions assemble molecules into a three-dimensional architecture, rather than the layers in **1**. Additional arene-C–H···S interactions, along the *c*-axis, also contribute to the stability of the overall molecular packing.

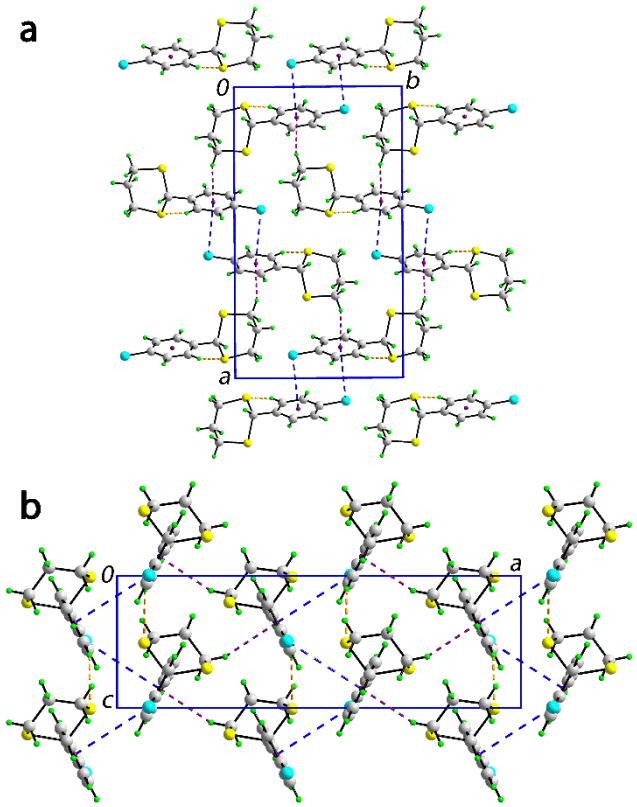

Fig. 5. (a) Two views of the unit cell contents for **2**: (a) down the *c*-axis, and b) down the *b*-axis, highlighting the similarly in the molecular packing with **1**. The methylene-C–H···π(arene), side-on C–Cl···π(arene) and arene-C–H···S interactions are shown as purple, blue and orange dashed lines, respectively.

In the molecular packing of **3**, only one specific interaction below accepted van der Waals radii assumed in PLATON [37] is noted. These are of the type methylene-C–H···π(arene) and lead to helical supramolecular chains, generated by a 2_1 screw axis along the *c*-axis, Fig. 6a. A methylene-C–H atom from a symmetry related molecule approaches the "unoccupied" face of the arene ring being separated by 3.12 Å from the ring centroid, Cg, i.e. beyond the normally accepts limits for C–H···π(arene) interactions [37]. Globally, chains assemble into undulating layers and stack along the *b*-axis.

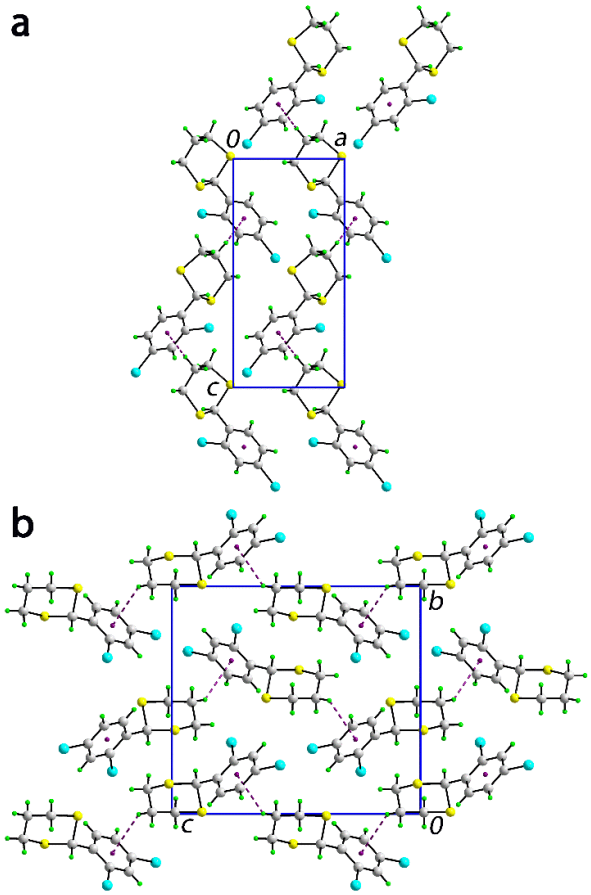

Fig. 6. Two views of the unit cell contents for **3**: (a) down the *b*-axis, highlighting the supramolecular helical chains, and b) down the *a*-axis. The C–H···π(arene) interactions are shown as purple dashed lines.

The packing arrangements in **1** and **2** are closely related whereby the methyl-C–H···π(arene) interactions of **1** are replaced by C–Cl···π(arene) interactions in **2**. However, the different orientation of the C–Cl···π(arene) interaction coupled with the additional C–H···S contact operating in the molecular packing of **2** ensure the structures are not isostructural. Allowing for the difference in β angles of ca 5º, the metric unit cell data for **1**, *abc*, approximates *bca* in **2**, Table 1. The molecular packing in **3**, although of a similar appearance, is quite distinct from **1** and **2**. The crystal packing efficiencies for **1**–**3**, computed with PLATON [37], amount to 64.8, 65.7 and 67.0%, respectively, and reflect the increasing unit cell density values, Table 1.

Based on the qualitative similarity in the global molecular packing in **1** and **2**, as highlighted in the pairs of diagrams, Figs 4a and 5a, and 4c and 5b, it was thought of interest to probe their relationship further. The first parameter calculated was Π,

$$\Pi = (a + b + c) / (a' + b' + c') - 1$$

where $(a + b + c) > (a' + b' + c')$ [58]. The calculation employs orthogonalised unit cell parameters which are generated automatically in PLATON [37]. Values of Π close to zero indicate a close match in unit cell parameters. In the

present case, Π computes to 0.56. Another parameter, namely the mean elongation, ε, was also investigated,

$$\varepsilon = (V'/V)1/3 - 1 \qquad (V' > V)$$

where, again, values close to zero indicate isostructurality [59]. For **1** and **2**, ε = 0.0075, the deviation confirming the structures are not isostructural.

Hirshfeld surface analysis

A further analysis of the molecular packing for **1**–**3** was made employing Hirshfeld surface analysis as this provides a convenient method for gaining useful information about the relative contribution of various intermolecular interactions to the overall molecular packing for a structure [60]; the present analysis was conducted with Crystal Explorer [61]. The overall fingerprint plots calculated for each of **1**–**3** are illustrated in Fig. 7, from which clear differences are apparent, consistent with different modes of supramolecular association between the molecules. Delineation of the fingerprint plots into specific interactions enables the relative contribution of each to the overall surface areas to be calculated; these are shown graphically in Fig. 8.

The most notable feature of the Hirshfeld surfaces for **1**–**3** is the relatively high contribution of hydrophobic H…H interactions in **1**, i.e. 62.3%, compared with 43.3 and 23.9%, respectively in **2** and **3**, indicating that each addition of Cl reduces the H…H contribution by approximately 20%; C–H···Cl interactions contribute 17.5 and 31.3% to the surfaces in **2** and **3**, respectively. The C–H···π(arene) interactions noted in the molecular packing of **1** contribute 16.5% to the overall surface area and this contribution is similar to 16.4 % in **2** and 19.0% in **3**. Also noteworthy is the observation that second most significant contribution to the overall surface area in **1**, at 20.5%, is due to C–H···S interactions even though these do not fall within the standard distance criteria [37]. Interestingly, this contribution is greater than 17.6% in **2**, where such an interaction is noted, and equivalent to 19.6% in **3**, where no specific C–H···S contact is formed. Finally, the C–Cl···π(arene) interaction commented upon in **2** corresponds to only 2.0% of the overall surface area; in **3**, this is 1.1%. In summary, the major differences in the overall Hirshfeld surface areas of **1**–**3** relate to the relative increase in contribution of C–H···Cl at the expense of H···H.

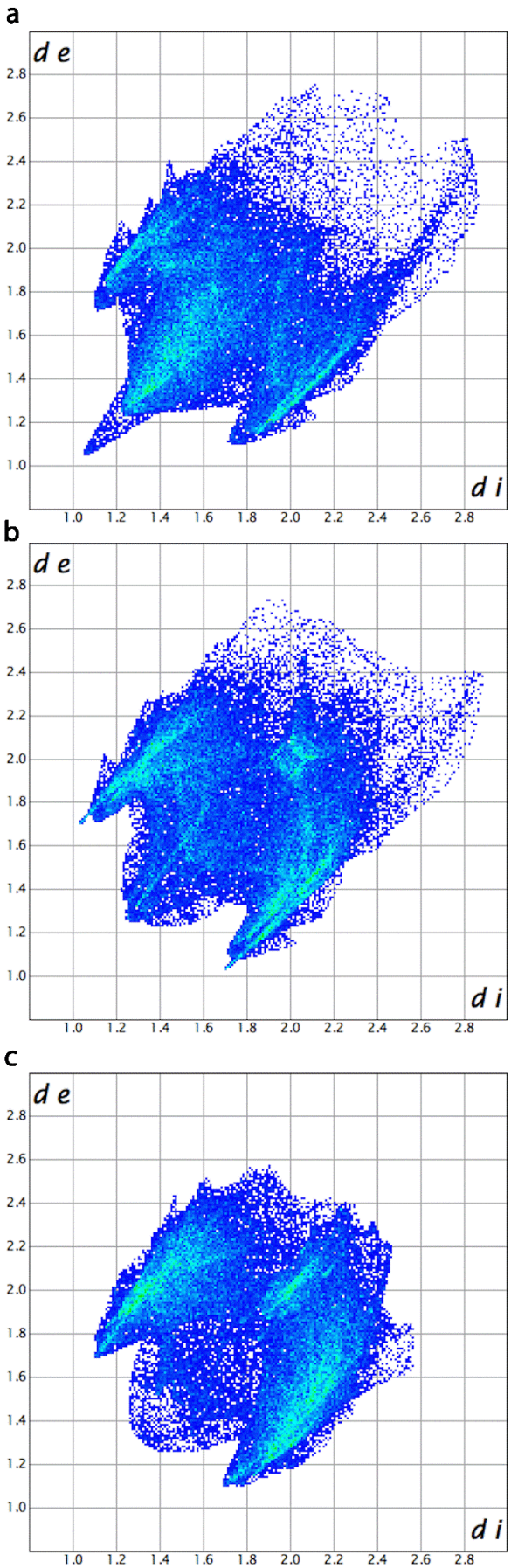

Fig. 7. Fingerprint (FP) plots for (a) **1**, (b) **2** and (c) **3**.

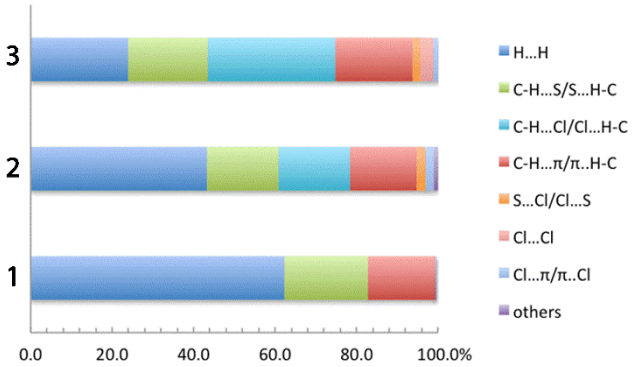

Fig. 8. Relative contributions of various intermolecular contacts to the Hirshfeld surface area in **1**–**3**.

Computational chemistry

A further analysis of **1**–**3** was conducted employing computational chemistry in order to gain insight into the observed molecular structures. Unrestrained geometry optimisation calculations were conducted. For each of **1** and **2**, the energy-minimised structures practically adopted almost identical conformations as seen in the experimental structures that practically had mirror symmetry, see Table 4. This is seen in the calculated root mean square deviations (RMSD) between the optimised and crystallographic structures of 0.01 and 0.03 Å, respectively. This situation is repeated for **3** where the RMSD between the observed and optimised structures was 0.01 Å. However, a second conformation may be envisaged for **3** which still retains the mirror symmetry, namely where the 2-chloride and methine-H atoms are anti, generated by a 180º rotation about the C2–C7 bond. Calculations showed the latter conformation to be less stable by approximately 4.0 kcal.mol^{-1}, an observation correlated with the formation of a favourable intramolecular C–H···Cl interaction in the most stable conformation as mentioned above.

Table 4. Relative energies (kcal.mol^{-1}) and torsion angles (°) of the optimised, experimental (crystallographic) and transition states molecular structures of **1**–**3**.[1]

	ΔG° (298.15 K)	ΔE_{ZPE}	ΔE	C12–C7–C2–H2
Optimised **1**	0.0	0.0	0.0	0.7
Experimental **1**	–	–	132.5	-3.1
Transition state **1**	4.9	3.5	3.4	88.2
Optimised **2**	0.0	0.0	0.0	0.7
Experimental **2**	–	–	109.3	-4.2
Transition state **2**	4.5	3.4	3.5	88.6
Optimised **3**	0.0	0.0	0.0	0.8
Experimental **3**	–	–	91.6	-8.9
Transition state **3**	13.3	11.8	12.1	95.2

[1] For the transition state conformations, ΔGº and ΔE are $\Delta G^{\#}$ and $\Delta E^{\#}$, respectively.

Next, the rotational barrier heights for **1**–**3** were investigated by fixing the dithiane ring in one position and rotating the arene ring about the C2–C7 bond, Table 4 and Fig. 9. For

1 and **2**, where rotation about the C2–C7 bond results in the same final conformation, the barrier to rotation was approximately 3.5 kcal.mol^{-1}. These values are in the same order of magnitude as rotation about a C–C single bond of common aliphatic hydrocarbons, even with carbon atoms bonded to bulky substituents [62-64].

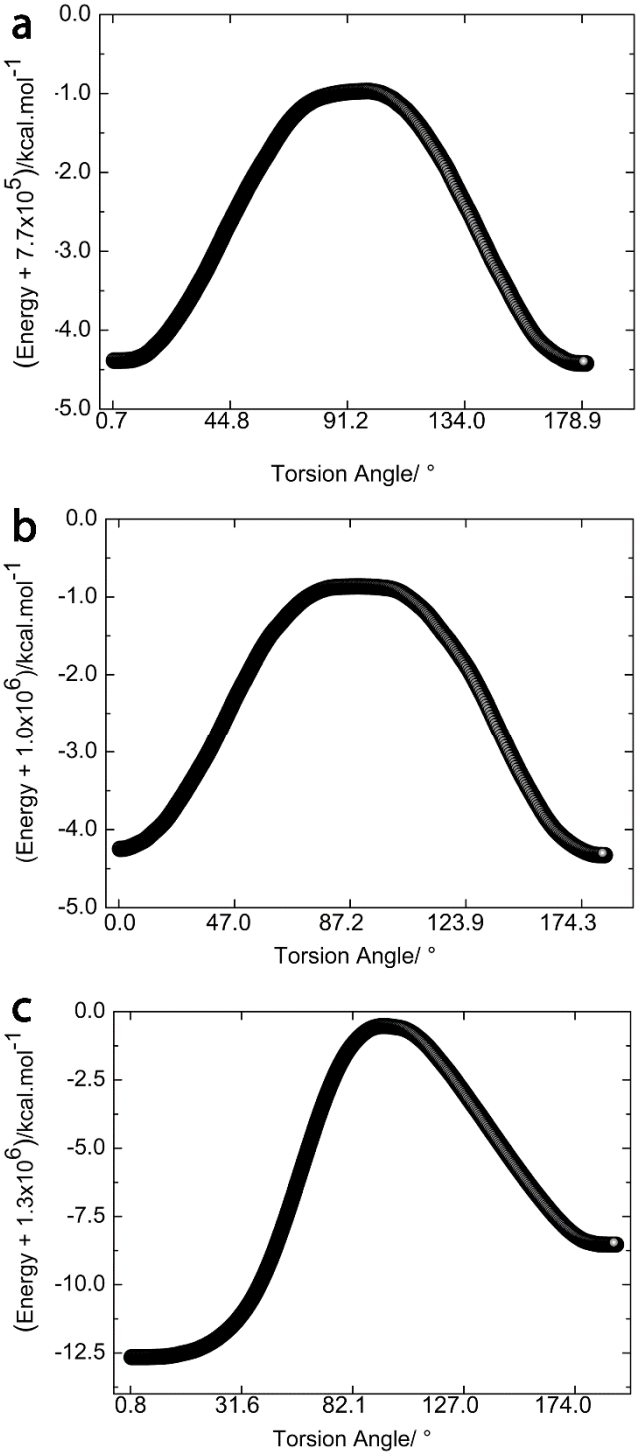

Fig. 9. Intrinsic reaction coordinate (IRC) profiles for (a) **1** (363 points), (b) **2** (378 points), and (c) **3** (437 points).

In order to evaluate the reasons for the energy barrier additional calculations were performed. The steric exchange

energies are collated in Table 5 and clearly indicate the instability induced in the molecule when the sulphur and ring carbon atoms are proximate, a situation which arises when the C12–C7–C2–H2 torsion angle is approximately 90º (Table 4).

Table 5. Major steric interactions between the aromatic and the dithiane rings in the molecular structures of **1**–**3**.

	Interaction	Steric exchange energy (kcal.mol^{-1})
Optimised **1**	H2…H12	1.4
Experimental **1**	H2…H12	0.9
Transition state **1**	S1...C12	3.2
	S3…C8	3.2
Optimised **2**	H2…H12	1.4
Experimental **2**	H2…H12	1.4
Transition state **2**	S1...C12	3.4
	S3…C8	3.4
Optimised **3**	–	0
Experimental **3**	–	0
Transition state **3**	S1…Cl114	5.9
	S3…C8	6.4

The energies associated with the hyperconjugation in this region of the molecules are collected in Table 6. These data suggest that hyperconjugation does not play a significant role in the activation energies as the $\pi_{C-C} \rightarrow \sigma^*_{C-H}$ and $\sigma_{C-H} \rightarrow \pi^*_{C-C}$ delocalisation in the transition states overcome the $\sigma_{C-C} \rightarrow \sigma^*_{C-H}$ and $\sigma_{C-C} \rightarrow \sigma^*_{C-C}$ delocalisation in the ground state conformations. It is also noted that in the transition states, favourable intramolecular H···S interactions are formed, i.e. 2 x -0.8 kcal.mol^{-1} for **1** and 2 x -0.9 kcal.mol^{-1} for **2**.

Table 6. Energies of selected hyperconjugative interactions in the molecular structures of **1**–**3**.

	Hyperconjugation	E2PRT (kcal.mol^{-1})
Optimised **1**	$\sigma_{C7-C8} \rightarrow \sigma^*_{C2-H2}$	-1.0
	$\sigma_{C2-H2} \rightarrow \sigma^*_{C7-C8}$	-5.5
Experimental **1**	$\sigma_{C7-C8} \rightarrow \sigma^*_{C2-H2}$	-0.7
	$\sigma_{C2-H2} \rightarrow \sigma^*_{C7-C8}$	-5.1
Transition state **1**	$\pi_{C7-C12} \rightarrow \sigma^*_{C2-H2}$	-3.3
	$\sigma_{C2-H2} \rightarrow \pi^*_{C7-C12}$	-4.0
Optimised **2**	$\sigma_{C7-C8} \rightarrow \sigma^*_{C2-H2}$	-1.0
	$\sigma_{C2-H2} \rightarrow \sigma^*_{C7-C8}$	-5.4
Experimental **2**	$\sigma_{C7-C8} \rightarrow \sigma^*_{C2-H2}$	-0.6
	$\sigma_{C2-H2} \rightarrow \sigma^*_{C7-C8}$	-5.8
Transition state **2**	$\pi_{C7-C12} \rightarrow \sigma^*_{C2-H2}$	-3.2
	$\sigma_{C2-H2} \rightarrow \pi^*_{C7-C12}$	-4.1
Optimised **3**	$\sigma_{C7-C8} \rightarrow \sigma^*_{C2-H2}$	-1.1
	$\sigma_{C2-H2} \rightarrow \sigma^*_{C7-C8}$	-5.3
Experimental **3**	$\sigma_{C7-C8} \rightarrow \sigma^*_{C2-H2}$	-0.8
	$\sigma_{C2-H2} \rightarrow \sigma^*_{C7-C8}$	-5.0
Transition state **3**	$\pi_{C7-C12} \rightarrow \sigma^*_{C2-H2}$	-2.5

	$\sigma_{C2–H2} \rightarrow \pi^*_{C7–C12}$	-4.5

The rotation barrier about the C2–C7 bond in **3**, i.e. approximately 12 kcal.mol^{-1}, is significantly greater cf. those in **1** and **2** (Table 4). This difference is related directly to the presence of the 2-chloride substituent which, when proximate to the sulphur atoms induces unfavourable interactions (Table 5), while at the same time removing the stabilising influence of the intramolecular H···Cl interactions formed in the ground state conformation where these atoms are syn (see above). It is also noted that the energies of the relevant hyperconjugative interactions in the ground state conformations are lower than in the transition state (Table 6).

A Natural Population Analysis (NPA) was conducted for the geometry optimised and experimental structures and the results collected in Table 7. It was of interest to ascertain whether any systematic variations in charge could be correlated with changing the electronegativity of the substituents in the aryl ring.

The first trend noted is that with respect to the experimental structures, greater charge residues on the non-hydrogen atoms than in the geometry-optimised structures. The second point to note is that there are no notable differences in the charges in the dithiane ring. Some trends are noted in the charges in the aryl ring with the most prominent being the increasing charge on C7 as the electronegativity of the substituents increases. This trend is accompanied by reduced charge on the C8 and C11 atoms. Finally, there is more charge on the C9 and C10 atoms in **2** and **3** cf. **1**. The above notwithstanding, the differences in charges are typically less than 0.03 so that any effects are small. These conclusions match those found in related studies where the electronegativity of substituents in aryl rings in small organic molecules were systematically varied [12, 13].

Table 7. Natural Population Analysis (NPA) for **1**-**3** calculated on the geometry-optimised and experimental (crystallographic) structures.

Atom	Opt. **1**	Expt'l **1**	Opt. **2**	Expt'l **2**	Opt. **3**	Expt'l **3**
S1	0.208	0.196	0.210	0.199	0.210	0.196
S3	0.208	0.199	0.210	0.203	0.210	0.200
C2	-0.475	-0.455	-0.473	-0.442	-0.471	-0.444
H2	0.209	0.178	0.210	0.178	0.230	0.195
C4	-0.507	-0.458	-0.506	-0.472	-0.506	-0.452
H4a	0.198	0.176	0.199	0.179	0.202	0.179
H4b	0.222	0.199	0.224	0.204	0.224	0.199
C5	-0.411	-0.364	-0.411	-0.360	-0.411	-0.363
H5a	0.207	0.189	0.209	0.190	0.210	0.191
H5b	0.212	0.191	0.213	0.190	0.213	0.191
C6	-0.507	-0.457	-0.506	-0.456	-0.506	-0.455
H6a	0.198	0.176	0.199	0.176	0.202	0.179
H6b	0.222	0.199	0.224	0.199	0.224	0.199
C7	-0.079	-0.044	-0.084	-0.054	-0.113	-0.112
C8	-0.178	-0.146	-0.166	-0.130	-0.150	-0.114
H8	0.221	0.182	0.227	0.187	0.232	0.189
C9	-0.202	-0.181	-0.223	-0.191	-0.227	-0.197
H9	0.203	0.170	0.224	0.187	0.228	0.190
C10	-0.023	0.021	-0.026	-0.012	-0.014	-0.001
C11	-0.207	-0.184	-0.227	-0.203	-0.252	-0.232
H11	0.203	0.170	0.224	0.189	0.239	0.201
C12	-0.168	-0.151	-0.158	-0.133	0.016	0.018
H12	0.204	0.172	0.210	0.175	–	–
C13	-0.597	-0.573	–	–	–	–
H13a	0.216	0.203	–	–	–	–
H13b	0.209	0.195	–	–	–	–
H13c	0.211	0.198	–	–	–	–
Cl13	–	–	-0.004	-0.002	0.008	0.012
Cl14	–	–	–	–	0.007	0.010

Discussion

From the foregoing despite similarities in conformation, global molecular packing and electronic structures, different modes of association operate in the crystal structures of **1**-**3**. A persistent supramolecular synthon is found in each of **1**-**3**, namely methylene-C–H…π(arene). In **1**, these are augmented by methyl-C–H…π(arene) interactions, and in **2** by C–Cl…π(arene) and C–H…S interactions. Interestingly, in the unsubstituted parent compound [53, 54], the unit cell symmetry most closely matches that of **2** but, the supramolecular association is related to that in **1**, featuring methyl- and methylene-C–H…π(arene) interactions. While this observation is consistent with a close relationship between the four crystal structures discussed herein, the subtle differences point to the significance of identified intermolecular interactions.

The crystal structures of **1** and **2**, differing only in the methyl and chloro substituents, presents the possibility of structural mimicry via the chloro/methyl exchange rule [7, 65]. Stated simply, if global crystal packing is the predominate factor determining the molecular packing, the exchange of a chloride with a methyl group, having similar volumes of 19 and 24 Å^3, respectively, should result in isostructural species. This concept breaks down in circumstances where one or the other of chloride or methyl engages in "significant" intermolecular interactions. In the present study, while these interactions are considered weak they are of sufficient strength and directionality to override the dictates of global crystal packing. Indeed, in the most comprehensive survey of the chloro/methyl exchange, it was found that in only 25% of the dataset where isostructurality could occur that it did [66].

Conclusions

Crystallography and computational chemistry indicate a high degree of conformational rigidity **1**-**3**, which approximate mirror symmetry in the solid-state, and that there is no significant influence exerted upon the electronic structures by the nature of the electron-donating methyl or electron-withdrawing chloro substituents. Despite the above, different molecular packing patterns are observed as confirmed by an analysis of the Hirshfeld surfaces. The lack of isostructural relationships, in particular between **1** and **2**, suggests that the identified intermolecular interactions are sufficiently structure directing in order to guide the supramolecular association between molecules.

Acknowledgements. We thank Professor Regina H. A. Santos from IQSC–USP for the X-ray data collection. The Brazilian agencies National Council for Scientific and Technological Development, CNPq, for scholarships (305626/2013-2 to J.Z.-S. and 308320/2010-7 to H.A.S.), São Paulo Research Foundation,

FAPESP, (2012/00424-2 and 2013/2192–2) and CAPES are acknowledged for financial support.

References

[1] M. C. Etter, *Acc. Chem. Res*. **1990**, *23*, 120.
[2] G. R. Desiraju, *Angew. Chem. Int. Ed*. **1995**, *34*, 2311.
[3] A. Priimagi, G. Cavallo, P. Metrangolo, G. Resnati, *Acc. Chem. Res*. **2013**, *46*, 2686.
[4] G. R. Desiraju, *J. Am. Chem. Soc*. **2013**, *135*, 9952.
[5] C. Janiak, *CrystEngComm* **2000**, *2*, 3885.
[6] M. Nishio, *CrystEngComm* **2004**, *6*, 130.
[7] J. D. Dunitz, A. Gavezzotti, *Acc. Chem. Res*. **1999**, *32*, 677.
[8] A. Gavezzotti, *CrystEngComm* **2013**, *15*, 4027.
[9] E. R. T. Tiekink, in Supramolecular Chemistry: from Molecules to Nanomaterials, J. W. Steed and P. A. Gale (eds), John Wiley & Sons Ltd, Chichester, UK, **2012**, pp. 2791.
[10] E. R. T. Tiekink, *Chem. Commun*. **2014**, *50*, 11079.
[11] R. Bishop, *CrystEngComm* **2015**, *17*, 7448.
[12] A. C. Cunha, V. F. Ferreira, A. K. Jordão, M. C. B. V. de Souza, S. M. S. V. Wardell, J. L. Wardell, P. A. Tan, R. P. A. Bettens, S. K. Seth, E. R. T. Tiekink, *CrystEngComm* **2013**, *15*, 4917.
[13] S. K. Seth, V. S. Lee, J. Yana, S. M. Zain, A. C. Cunha, V. F. Ferreira, A. K. Jordão, M. C. B. V. de Souza, S. M. S. V. Wardell, J. L. Wardell, E. R. T. Tiekink, *CrystEngComm* **2015**, *17*, 2255.
[14] E. J. Corey, D. Seebach, *Angew. Chem., Int. Ed. Engl*. **1965**, *4*, 1075.
[15] D. Seebach, E. J. Corey, *J. Org. Chem*. **1975**, *40*, 231.
[16] D. Seebach, *Synthesis* **1969**, 17.
[17] B. T. Grobel, D. Seebach, *Synthesis* **1977**, 357.
[18] P. C. B. Page, M. B. van Niel, J. C. Prodger, *Tetrahedron* **1989**, *45*, 7643.
[19] M. Yus, C. Najera, F. Foubelo, *Tetrahedron* **2003**, *59*, 6147.
[20] A. B. Smith III, C. M. Adams, *Acc. Chem. Res*. **2004**, *37*, 365.
[21] A. B. Smith III, D.-S. Kim, *J. Org. Chem*. **2006**, *71*, 2547.
[22] H. A. Stefani, R. Cella, J. Zukerman-Schpector, I. Caracelli, Z. *Kristallogr. NCS* **2006**, *221*, 167.
[23] I. Caracelli, H. A. Stefani, A. S. Vieira, M. M. P. Machado, J. Zukerman-Schpector, Z. *Kristallogr. NCS* **2007**, *222*, 345.
[24] A. S. Vieira, F. P. Ferreira, P. F. Fiorante, R. C. Guadagnin, H. A. Stefani, *Tetrahedron* **2008**, *64*, 3306.
[25] R. Cella, R. L. O. R. Cunha, A. E. S. Reis, D. C. Pimenta, C. F. Klitzke, H. A. Stefani, *J. Org. Chem*. **2006**, *71*, 224.
[26] R. Cella, H. A. Stefani, *Tetrahedron* **2006**, *62*, 5656.
[27] H. A. Stefani, R. Cella, F. A. Dörr, C. M. P. Pereira, G. Zeni, M. Gomes Jr, *Tetrahedron Lett*. **2005**, *46*, 563.
[28] R. Cella, A. T. G. Orfão, H. A. Stefani, *Tetrahedron Lett.* **2006**, *47*, 5075.
[29] R. Cella, R. C. Venturoso, H. A. Stefani, *Tetrahedron Lett.* **2008**, *49*, 16.
[30] K. Kazahaya, S. Tsuji, T. Sato, *Synlett* **2004**, 1640.
[31] H. R. Shaterian, A. Hosseinian, M. Ghashang, F. Khorami, *Phosphorus, Sulfur and Silicon and the Related Elements* **2008**, *183*, 2490.
[32] Bruker. APEX2 and SAINT. Bruker AXS Inc., Madison, Wisconsin, USA, **2009**.
[33] G. M. Sheldrick. SADABS. University of Göttingen, Germany, **1996**.

[34] M. C. Burla, R. Caliandro, B. Carrozzini, G. L. Cascarano, C. Cuocci, C. Giacovazzo, M. Mallamo, A. Mazzone, G. Polidori, *J. Appl. Cryst*. **2015**, *48*, 306.
[35] G. M. Sheldrick, *Acta Crystallogr. C* **2015**, *71*, 3.
[36] L. J. Farrugia, *J. Appl. Crystallogr*. **2012**, *45*, 849.
[37] A. L. Spek, *Acta Crystallogr. D* **2009**, *65*, 148.
[38] J. Gans, D. Shalloway, *J. Mol. Graph. Model*. **2001**, *19*, 557.
[39] DIAMOND, Visual Crystal Structure Information System, Version 3.1, CRYSTAL IMPACT, Postfach 1251, D-53002, **2006**.
[40] A. A. Granovsky, Firefly, version 8; http://classic.chem.msu.su/gran/firefly/index.htm
[41] M. W. Schmidt, K. K. Baldridge, J. A. Boatz, S. T. Elbert, M. S. Gordon, J. H. Jensen, S. Koseki, N. Matsunaga, K. A. Nguyen, S. Su, T. L. Windus, M. Dupuis, J. A. Montgomery, *J. Comput. Chem*. **1993**, *14*, 1347.
[42] A. D. Becke, *J. Chem. Phys*. **1993**, *98*, 5648.
[43] R. Krishnan, J. S. Binkley, R. Seeger and J. A. Pople, *J. Chem. Phys.* **1980**, *72*, 650.
[44] A. D. McLean, G. S. Chandler, *J. Chem. Phys*. **1980**, *72*, 5639.
[45] T. Clark, J. Chandrasekhar, G. W. Spitznagel, P. V. R. Schleyer, *J. Comp. Chem.* **1983**, 4, 294.
[46] F. Jensen. *J. Chem. Phys*., **1995**, *102*, 6706.
[47] C. Gonzalez, H. B. Schlegel, *J. Chem. Phys.* **1991**, *95*, 5853.
[48] G. E. D. Glendening, J. K. Badenhoop, A. E. Reed, J. E. Carpenter, J. A. Bohmann, C. M. Morales, F. Weinhold, NBO 5. Theoretical Chemistry Institute, University of Wisconsin, Madison, WI, **2004**; http://www.chem.wisc.edu/~nbo5
[49] B. M. Bode, M. S. Gordon, *J. Mol. Graph. Model.* **1998**, *16*, 133.
[50] JMol: An open-source Java viewer for chemical structures in 3D. http://www.jmol.org/
[51] P. G. Jene, J. A. Ibers, *Acta Crystallogr. C* **2000**, *56*, 705A.
[52] J. Adamson, R. E. Banks, K. N. Mothersdale, R. G. Pritchard, T. Manley, A. E. Tipping, *Acta Crystallogr. C* **1995**, *51*, 772.
[53] H. T. Kalff, C. Romers, *Acta Crystallogr*. **1966**, *20*, 490.
[54] G. Adiwidjaja, T.-Y. Luh, J. Voss, J. Wirsching, *Private Communication to the Cambridge Structural Database*, **2003**.
[55] H.-K. Fun, R. Kia, A. C. Maity, S. Goswami, *Acta Crystallogr. E* **2009**, *65*, o348.
[56] J. Zukerman-Schpector, I. Caracelli, H. A. Stefani, O. Gozhina, E. R. T. Tiekink, *Acta Crystallogr. E* **2015**, *71*, o179.
[57] I. Caracelli, J. Zukerman-Schpector, H. A. Stefani, O. Gozhina, E. R. T. Tiekink, *Acta Crystallogr. E* **2015**, *71*, o181.
[58] A. Kálmán, L. Párkányi, Gy. Argay, *Acta Crystallogr. B* **1997**, *49*, 1039.
[59] J. S. Rutherford, *Acta Chim. Hung*. **1997**, *134*, 395.
[60] A. L. Rohl, M. Moret, W. Kaminsky, K. Claborn, J. J. Mackinon, B. Kahr, *Cryst. Growth Des*. **2008**, *8*, 4517.
[61] S. K. Wolff, D. J. Grimwood, J. J. McKinnon, M. J. Turner, D. Jayatilaka, M. A. Spackman, Crystal Explorer (Version 3.1), University of Western Australia, **2012**.
[62] P. M. Schreiner, *Angew. Chem. Int. Ed.* **2002**, *41*, 3579.
[63] Y. Mo, W. Wu, L. Song, M. Lin, Q. Zhang, J. Gao, *Angew. Chem. Int. Ed*. **2004**, *43*, 1986.
[64] R. M. Pitzer, *Acc. Chem. Res*. **1983**, *16*, 207.

[65] G. R. Desiraju, J. A. R. P. Sarma, *Proc. Ind. Acad. Sci. (Chem. Sci.)* **1986**, *96*, 599.
[66] J. van de Streek, W. D. S. Motherwell, *J. Appl. Crystallogr.* **2005**, *38*, 694.